Phys. Status Solidi C **11**, No. 3–4, 381–384 (2014) / **DOI** 10.1002/pssc.201300460

physica status solidi c
www.pss-c.com
current topics in solid state physics

InGaN doping for high carrier concentration in plasma-assisted molecular beam epitaxy

Iulian Gherasoiu[*,1,3], Kin Man Yu[,2], Lothar A. Reichertz[1,2], and Wladek Walukiewicz[1,2]**

[1] RoseStreet Labs Energy, Phoenix, AZ, USA
[2] Materials Sciences Division, Lawrence Berkeley National Laboratory, Berkeley, CA, USA
[3] Element Blue Technology, Phoenix, AZ, USA

Received 22 August 2013, revised 29 September 2013, accepted 29 November 2013
Published online 28 January 2014

Keywords InGaN, GaN, doping, LED

* Corresponding author: e-mail igherasoiu@elementbluetech.com
** e-mail kmyu@lbl.gov

Magnesium is the only known effective p-type dopant for nitride semiconductors. Although the p-doping is challenging for AlN and GaN, requiring the activation of the Mg acceptors, in the case of the MOCVD growth, methods for obtaining reliable and high level doping have been developed. Similarly for n-type doping silicon has been used successfully for more than a decade. More recently germanium has been found to be as effective for n-type doping, with the additional advantage of inducing less strain in the host lattice due its size similarity to gallium. Doping of InGaN is more challenging due the difficulty in controlling the donor background associated with material extended defects and the incorporation of impurities. Although successful p-type doping of InGaN with Mg has been demonstrated, quantitative limits for the magnesium incorporation and its behavior have not been analyzed. In this paper we investigate both, Mg and Ge doping of InGaN. We also discuss the challenges posed by the growth and measurement of the InGaN pn-junctions characteristics as well as we demonstrate the fabrication of large area long wavelength LEDs on silicon (111) by PA-MBE.

1 Introduction InGaN semiconductors have a direct band gap spanning from 0.7 eV to 3.4 eV. This band gap could allow the fabrication of solar cells converting the energy across entire solar spectrum [1, 2]. However, further improvements regarding the material growth and doping are required in order to increase the conversion efficiency to practically significant levels. Recently we have reported on the progress growing InGaN with indium fractions larger than 20% and on the photovoltaic action from such structures [3, 4]. Optimized multi-junction solar cells require the incorporation of larger indium fractions. For this reason, the InGaN alloys have been subject of sustained work targeting the synthesis of layers with high crystalline quality and high indium fraction (>30%) that would allow the absorption of light with longer wavelengths from the solar spectrum.

Doping of such material is required in order to enable efficient charge carrier generation and collection. Therefore, we have determined the upper Mg doping concentrations for GaN and InGaN with large indium fractions. Below this limit, high acceptor concentrations and efficient doping can be established. We have also determined the effect of Ge incorporation on the electron concentration and mobility, in InGaN with indium fractions between 32% and 40%. Ultimately we discuss and demonstrate the fabrication of large area green and yellow InGaN LEDs on Si (111) substrates.

2 Experimental We have grown GaN and InGaN films on 2 inch GaN/sapphire templates using a production-style plasma-assisted molecular beam epitaxy (PA-MBE) system equipped with Veeco UNI-Bulb RF plasma sources. The insulating GaN templates were grown by MOCVD and had a nominal thickness of 5 µm. The growth was initiated by depositing 200 nm of nominally un-doped GaN. The magnesium doped layers of GaN have a thickness in the range from 550 nm to 850 nm while the thickness of the InGaN layers is of 300 nm. All InGaN films have been grown at the same substrate temperature

and using the same indium flux. Mg cell temperature was increased such that the beam equivalent pressure (BEP) at the sample surface ranged from ~1x10^{-9} Torr to 1.6x10^{-7} Torr.

Film composition and thickness were evaluated by Rutherford backscattering spectrometry (RBS) and secondary ion mass spectrometry (SIMS), while the crystallinity of the film was evaluated using ion channelling. Hall and electrochemical capacitance voltage (ECV) measurements were used to estimate the conduction type, carrier density and mobility. SIMS analysis was used to investigate the dopant (Mg and Ge) distribution and density.

3 Results and discussion The effect of magnesium incorporation on GaN and $In_xGa_{1-x}N$ layers with high indium fraction (x=0.4) was investigated. In Fig. 1 the dependence of the ion channelling yield on the density of Mg atoms incorporated is presented. Low values of the channelling yield are associated with high crystalline quality while larger values suggest a higher scattering rate of the ions due lattice imperfections. The black filled symbols represent the crystallinity at the surface of the GaN:Mg layer while the red, open symbols represent the crystallinity of the GaN:Mg layer 500 nm below the layer's surface. There is a noticeable and linear decrease of the ion channelling yield at surface when compared with the value at 500 nm, suggesting that the crystallinity of the layer improves gradually, as the thickness increases, by almost an order of magnitude. The plot reveals that for a Mg concentration larger than 6-7x10^{20} cm^{-3}, the crystallinity of GaN film deteriorates. The samples incorporating larger amounts of Mg exhibit a channelling yield that is approximately one order of magnitude larger than that of the samples having Mg densities below this threshold. The measurements of the carrier properties performed using Hall method (density, mobility and conduction type) are correlated with respect to this threshold as well. Below the threshold concentration the measured samples exhibit p-type conduction. For concentrations of Mg in the 10^{20}cm^{-3} range, we have measured hole concentrations in the range from 2.2x10^{18}cm^{-3} to 4x10^{18}cm^{-3} and low carrier mobilities (1.9-2.6 cm^2/Vs), while larger mobilities (10-12 cm^2/Vs) are associated with lower hole concentration (3.75x10^{17}-4x10^{17}cm^{-3}) and lower Mg concentration (10^{18}-10^{19}cm^{-3}). Above the threshold the conduction is dominated by the conduction band electrons (n-type) with concentrations around 1x10^{18} cm^{-3} and mobilities of 152 cm^2/Vs and 93 cm^2/Vs, respectively. The activation efficiency of the Mg acceptors appears to be dependent on the Mg concentration as well. At low Mg concentration the activation efficiency is of ~10% and decreases quickly with the increase of the Mg concentration, reaching 0.7% for the samples near the conduction type threshold.

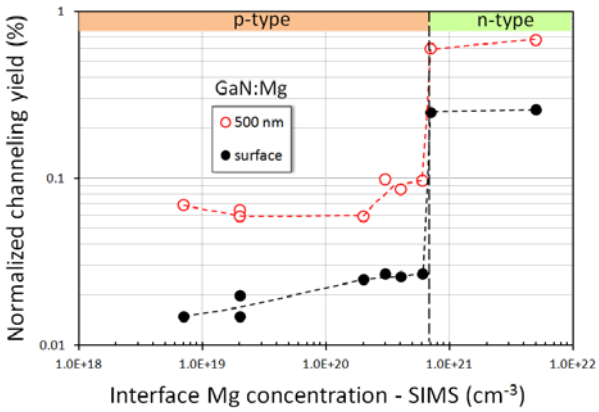

Figure 1 Dependence of the ion channelling yield on the magnesium concentration in GaN films as determined by SIMS.

The change in the conductivity type is clearly associated with an increase in the ion scattering events as measured by the increase of the channelling yield value. The formation of donor-type defects is likely the cause for the change in the conductivity type but the identification of the nature of the defect was not within the scope of this study. It has been found that besides nitrogen vacancies (V_N), the Mg_{Ga}-V_N vacancy complex has also a donor character contributing to the acceptor compensation in p-type GaN [5]. In a previous study regarding the p-doping of MOCVD GaN [6], a Mg incorporation limit of 3x10^{19}cm^{-3} has been found which is approximately one order of magnitude lower than that of PA-MBE GaN. A similar change of the film conductivity with the increase of the Mg flux was reported for the doping of $In_xAl_{1-x}N$, [7].

In the case of InGaN films the channelling yield depends not only on the impurity incorporation but also increases with the fraction of indium, for the $In_xGa_{1-x}N$ composition range with $0<x<0.5$. Therefore the channelling yield is not an accurate representation of the magnesium incorporation. The conductivity type of the epitaxial layer is also challenging to determine especially for InGaN alloys with indium fractions larger than 35%. For these higher indium fraction alloys, the surface of the film accumulates electrons as the Fermi level becomes pinned above the conduction band edge. In this case the magnesium incorporation limit was determined based on the competition between In and Mg for the InGaN lattice site. Magnesium has to occupy the lattice site of the group III element in order to form an acceptor. Therefore, it is expected that magnesium would gradually replace some of indium in the lattice places of the group III element, as its concentration increases. However, we have found a behaviour that is characterized by a threshold with respect to indium incorporation, Fig. 2. For Mg fluxes (BEP) larger than 1x10^{-7} Torr, indium incorporation is prevented to a large extent and the formation of a quaternary $In_xMg_yGa_{1-x-y}N$ alloy with $0.12>y>0.06$ and $0.01>x>0.004$ is observed.

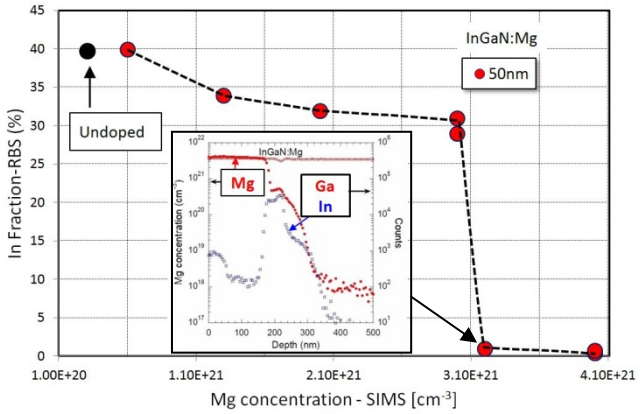

Figure 2 Dependence of the indium fraction of the magnesium concentration in $In_xGa_{1-x}N$ films with x=0.4, as determined by SIMS. The insert depicts the SIMS analysis of a quaternary $In_xMg_yGa_{1-x-y}N$ film with y=0.12 and 0.005>x>0.001.

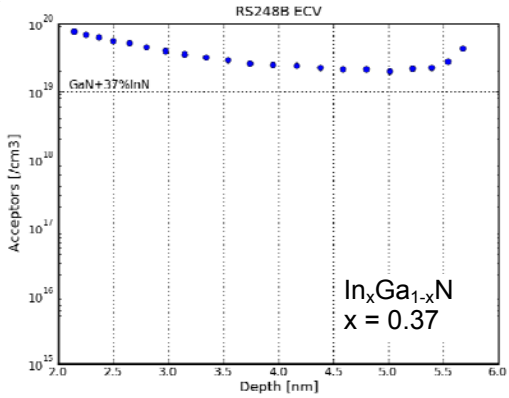

Figure 3 Net ionized Mg acceptor density measured by ECV. The depth represents the depletion region distance from the surface of the sample.

The SIMS elemental concentration profile of such a quaternary alloy sample is presented in the insert of the Fig. 2.

It is noticeable that after an initial growth regime characterized by the incorporation of a relatively high fraction of indium, the Mg incorporation has a sudden increase while indium concentration falls by more than 2 orders of magnitude. We infer that the behaviour relates to the surface accumulation of Mg and its preferential incorporation over that of indium. It is worth noting that Hall measurements of the InMgGaN layers find n-type conductivity with an electron concentration of ~$9x10^{18}$ cm^{-3} and mobility of 189 cm^2/Vs. More details regarding the material structure and properties will be provided elsewhere.

To avoid the accumulation of Mg at the growth surface, the arrival of the participating atomic species has been controlled by the coordination of the shutter opening. Thus Mg has been admitted in the chamber while the group III shutters were closed. Using this technique we have been able to obtain extremely high densities of ionized Mg acceptors (net concentration) in the range from $2x10^{19}$ cm^{-3} to $8x10^{19}$ cm^{-3} for InGaN layers with indium fractions as high as 37%, as measured by ECV, Fig. 3. Previous work, [8] has found a hole concentration at room temperature of $1.7x10^{19}$ cm^{-3} for InGaN with an indium fraction of 29%. The activation energy found by the authors, for InGaN with 17% indium fraction is of only 48 meV. This energy is expected to reduce further with the increase of the indium fraction and we consider that at a fraction of 37%, the density of ionized acceptors is roughly equal with the density of hole carriers.

Germanium has been used successfully as n-type dopant replacing silicon. We have found that for Ge concentrations from $1x10^{20}cm^{-3}$ up to ~$4.5x10^{20}$ cm^{-3}, the electron concentration increases exponentially with the increase of the Ge doping. This is also reflected in the activation efficiency that increases from 5% at the lowest Ge concentration, up to 85% for the Ge concentration of $4.5x10^{20}cm^{-3}$, Fig. 4. At this level, the electron concentration saturates at maximum of $3.9x10^{20}$ cm^{-3}, and any further increase in Ge concentration appears to generate lattice defects that tend to compensate the electron carriers.

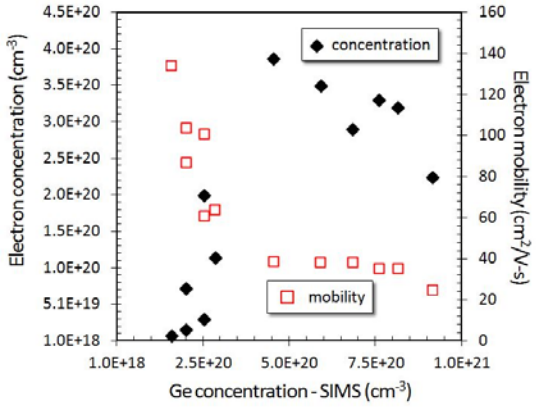

Figure 4 Dependence of electron carrier properties on the germanium concentration in GaN films as determined by SIMS.

The highest electron mobility, 134 cm^2/Vs is obtained for the lowest Ge concentration and similar with the electron density, the electron mobility saturates around 40 cm^2/Vs, for the same range of Ge concentrations.

In the case of Ge-doped InGaN, with indium fractions between 32% and 40%, the highest electron concentration measured was $7.4x10^{20}$ cm^{-3} for a concentration of Ge of $4x10^{20}$ cm^{-3}, Fig. 5. This is not unexpected since for this range of indium fractions electrons are known to accumulate at the surface. The Hall measured value would thus reflect the transport properties of the surface electrons as well as those of the bulk electrons. For the InGaN layers, the measured mobility ranged from 88 cm^2/Vs to 25 cm^2/Vs, with the higher mobility corresponding to an electron concentration of $1.6x10^{19}$ cm^{-3}.

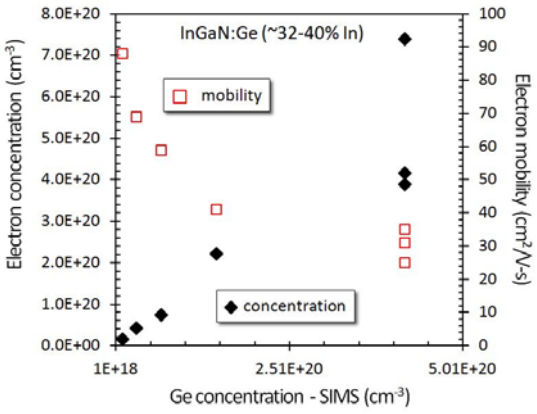

Figure 5 Dependence of electron carrier properties on the germanium concentration in InGaN films, as determined by SIMS.

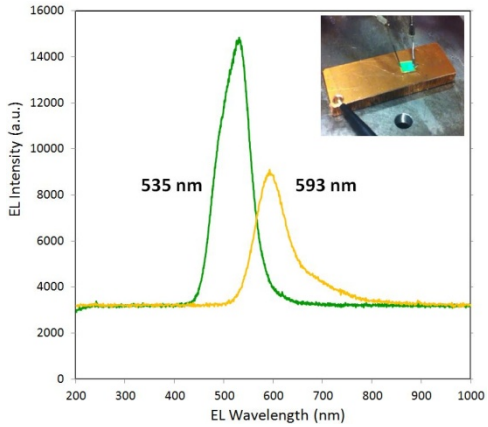

Figure 6 Room temperature EL spectra of InGaN green and yellow LEDs under 10 mA pulsed current. The optical view of the RT green emission of (5x5) mm InGaN LED.

Furthermore, we have grown layers of AlN/n-GaN/n-InGaN/p-InGaN/p-GaN on p-silicon (111). The n-GaN was grown under 2-dimensional growth mode while the n-InGaN layers were grown under N-rich conditions, allowing the on-set of Stranski-Krastanov growth mode. Finally, graded p-InGaN and p-GaN layers have been grown under metal-rich conditions to promote faster lateral growth.

We have used two different samples to define small structures and measure the electroluminescence. The two samples emit light at 535 nm and 593 nm, respectively, under 10 mA pulsed current (1 kHz, 50%), as presented in Fig. 6. Photolithography and electron beam evaporation were then used to deposit a Ni/Au grid on the top p-type GaN layer. Electron beam evaporation was also used to deposit Ti/Pd/Ag onto the back side of the Si wafer to form the back ohmic contact of these structures with a surface of 0.25 cm^2. The sample was held down on a copper block and under bias allowing a current density of ~1 A/cm^2, green emission was observed over the entire area of the sample, insert of Fig. 6.

Long wavelength LEDs have been grown in the past based on structures using the formation of multi-quantum disks, or quantum dots imbedded in nano-columns [9] or quantum wells [10], respectively. When the indium fraction of the emission regions is increased, a strong decrease in the light output intensity is observed and reported [9, 10, 11]. In the case of our structures, the output intensity decreased by almost 40% for the yellow LED when compared with the green LED. One explanation proposed the quantum confined Stark effect (QCSE) for the light red-shift and reduced radiation efficiency [11].

Our photovoltaic experiments suggest that the current forward leakage along the threading dislocations becomes the main carrier loss mechanism in un-doped InGaN layers with indium fractions around 35%, due to the decrease of the potential energy barrier that is screening the lattice defects at lower indium fractions.

4 Conclusions Mg and Ge doping behaviour of $In_xGa_{1-x}N$ with x>30% has been analyzed. We have devised techniques allowing the achievement of high carrier concentrations and determined practical limits for the incorporation of these dopants. Relatively large area LED structures have been fabricated from which green and yellow electro-luminescence has been measured.

Acknowledgements This work was supported by Rose-Street Energy Laboratory, Contract LB07003462 and U.S. DOD/DARPA under contract W91CRB-11-C-0012.

References

[1] J. Wu, W. Walukiewicz, K. M. Yu, W. Shan, J. W. Ager III, E. E. Haller, H. Lu, W. J. Schaff, W. K. Metzger, and S. Kurtz, J. Appl. Phys. **94**, 6477 (2003).
[2] J. W. Ager III, J. Wu, K. M. Yu, R. E. Jones, S. X. Li, W. Walukiewicz, E. E. Haller, Hai Lu, and W. J. Schaff, 4th Int. Conference on Solid State Lighting, edited by I. T. Ferguson, N. Narendran, S. P. DenBaars, and J. C. Carrano, Proc. SPIE **5530** (SPIE, Bellingham, WA, 20 Oct. 2004).
[3] I. Gherasoiu, K. M. Yu, L. A. Reichertz, V. M. Kao, M. Hawkridge, J. W. Ager III, and W. Walukiewicz, Phys. Status Solidi B **247**(7), 1747 (2010).
[4] I. Gherasoiu, L. A. Reichertz, K. M. Yu, J. W. Ager III, V. M. Kao, and W. Walukiewicz, Phys. Status Solidi C **8**(7-8), 2466 (2011).
[5] Q. Yan, A. Janotti, M. Scheffler, and C. G. Van de Walle, Appl. Phys. Lett. **100**, 142110 (2012).
[6] H. Obloh, K.H. Bachem, U. Kaufmann, M. Kunzer, M. Maier, A. Ramakrishnan, and P. Schlotter, J. Cryst. Growth **195**(1-4), 270 (1998).
[7] K. D. Matthews, X. Chen, D. Hao, W. J. Schaff, and L. F. Eastman, Phys. Status Solidi C **5**(6), 1863 (2008).
[8] D. Iida, M. Iwaya, S. Kamiyama, H. Amano, and I. Akasaki, Appl. Phys. Lett. **93**, 182108 (2008).
[9] A. Kikuchi, M. Tadaa, K. Miwaa, and K. Kishinoa, Proc. SPIE **6129**, 612905 (2006).
[10] T. Xu, A. Y. Nikiforov, R. France, C. Thomidis, A. Williams, and T. D. Moustakas, Phys. Status Solidi A **204**(6), 2098 (2007).
[11] T. Mukai, M. Yamada, and S. Nakamura, Jpn. J. Appl. Phys. **38**, 3976 (1999).

